BULLETIN OF THE POLISH ACADEMY OF SCIENCES
TECHNICAL SCIENCES, Vol. 74(6), 2026, Article number: 3058
DOI: 10.24425/bpasts.2026.3058

Quantum-enhanced physics-informed neural network framework for multi-modal optimization of diffractive optics in extreme laser environments

R. Hariharan[1], N. Prathap[2]*, M. Irshad Ahamed[3], M. Nuthal Srinivasan[3]

[1] Department of Electronics and Communication Engineering, University College of Engineering, Thirukkuvalai, Tamil Nadu, India
[2] Department of Electronics and Communication Engineering, Anjalai Ammal Mahalingam Engineering College, Kovilvenni, Tamil Nadu, India
[3] Department of Electronics and Communication Engineering, E.G.S. Pillay Engineering College, Nagapattinam, Tamil Nadu, India

Abstract. Q-PINN-opt creates a new framework by combining the concepts of quantum computing with Physics-Informed Neural Networks (PINNs) for multi-modal optimization of diffractive optics under laser conditions. In high-power laser applications, which involve the optimization of complex problems, the model employs quantum-enhanced optimization coupled with physics-informed learning. In contrast to traditional approaches based on PINNs or Wiener filters, which are limited by their inability to scale, poor computational efficiency, and limited resilience to extreme conditions, Q-PINN-opt is a hybrid quantum-classical algorithm that accelerates convergence and maximizes computational efficiency. The major innovation of the Q-PINN-opt variant is that quantum algorithms (such as Quantum Gradient Descent and Quantum Approximate Optimization Algorithm (QAOA)) are implemented using classical PINNs. This enables faster, scalable, and multimodal optimization of problems, including diffraction efficiency, phase accuracy, and resistance to thermal, nonlinear, and quantum-induced effects. Current models such as PINNs may also exhibit slow convergence and computational inefficiency when applied to optimization problems of a complex, high-dimensional nature, especially when multiple performance criteria are to be optimized simultaneously. Q-PINN-opt addresses all these shortcomings; thus, it is specifically applicable to the optimization of diffractive optics for real-time adaptive learning. Q-PINN-opt addresses this problem by leveraging quantum computing to train more effectively and process large-scale data efficiently. Moreover, the hybrid quantum-classical model ensures the physical constraints of network solutions, enhancing the resilience and scalability of high-performance optical systems. The Q-PINN-opt framework metric analysis reveals that it performs better than other models. MSE, SSIM, and SNR in the model are 6.84, 0.99, and 7.98, respectively, which implies that the model has high accuracy, diffraction efficiency, and resistance to noise. In contrast, the original model achieves an MSE of 9.55 and an SNR of 5.54. The improvements enhance both the training and the convergence of the optimization, making Q-PINN-opt well-constructed and efficient for the design of complicated diffractive optics in extreme environments.

Keywords: quantum computing; Physics-Informed Neural Networks (PINNs); multi-modal optimization; diffractive optics; hybrid quantum-classical approach; laser optimization.

1. INTRODUCTION

The Quantum-Enhanced Physics-Informed Neural Network Optimization framework (Q-PINN-opt) is proposed in this study as an advanced hybrid quantum-classical approach for solving complex optimization problems in diffractive optics under extreme laser environments. Diffractive optical elements (DOEs) play a key role in modern optical systems because they allow precise manipulation of light for beam shaping, laser focusing, optical communication, and high-energy laser applications. In extreme laser environments, however, the design of DOEs becomes highly challenging. The optical response is affected by nonlinear material behavior, geometric variations, phase modulation errors, thermal loading, vibration, and laser-induced perturbations. As a result, DOE optimization often becomes a nonlinear and high-dimensional problem that requires both physical accuracy and computational efficiency [1–4].

Physics-Informed Neural Networks (PINNs) have emerged as a useful approach for solving complex physical problems because they embed governing equations directly into the learning process. Instead of relying only on data, PINNs incorporate physical constraints, such as Maxwell's equations, into the loss function so that the predicted solution remains physically meaningful [5,6]. Recent studies have further demonstrated the value of PINN-based models for improving physical consistency, interpretability, and convergence in complex engineering systems. In particular, PINN formulations have been theoretically and numerically validated for structural dynamic response analysis by incorporating governing equation residuals into the training process [7]. In another recent development, physics-informed Kolmogorov–Arnold network architectures have shown the ability to learn meaningful high-dimensional representations while retaining interpretability and prediction accuracy [8]. Similarly,

*e-mail: prathap27n@gmail.com

Manuscript submitted 2026-03-11, revised 2026-05-13, initially accepted for publication 2026-08-03, published in November 2026.

© 2026 The Author(s). This is an open access article under the CC BY license (http://creativecommons.org/licenses/by/4.0/)

label-free PINNs with hard physical constraints and Fourier feature spectral enhancement have improved convergence in multi-frequency nonlinear dynamic systems [9]. These developments are relevant to diffractive-optics optimization because the present problem also requires simultaneous consideration of electromagnetic field behavior, phase accuracy, diffraction efficiency, and robustness under thermal and vibrational disturbances.

Although PINNs provide a strong physics-guided learning framework, conventional PINN models may still experience slow convergence and limited efficiency when the optimization space is large, nonlinear, and multi-modal. This limitation becomes more evident in DOE design, where several performance objectives must be optimized at the same time. To address this issue, the proposed Q-PINN-opt framework combines PINN-based physical constraint enforcement with quantum-assisted optimization strategies, including parameterized quantum circuits, quantum-gradient-based learning, and hybrid quantum-classical optimization [10, 11]. In this structure, the quantum layer supports broader exploration of the design space, while the PINN component ensures that the predicted optical fields remain consistent with the underlying electromagnetic physics.

The proposed Q-PINN-opt framework is designed for multi-modal optimization of DOEs under extreme laser conditions. It jointly considers diffraction efficiency, phase accuracy, focal spot control, thermal robustness, and resistance to external perturbations [12, 13]. By combining the search capability of quantum-assisted optimization with the physical interpretability of PINN-based learning, the framework aims to improve convergence behavior, solution stability, and computational scalability. This makes it suitable for the design of high-performance optical components that must operate reliably under high thermal loads, vibration, and laser-induced distortion [14–16].

Key contribution

- Quantum computing integration: Introduces a novel approach that incorporates quantum computing into diffractive-optics design for high-power laser applications.
- Q-PINN-Opt framework: Proposes the Quantum-Enhanced Physics-Informed Neural Network (Q-PINN-Opt) framework to solve multi-modal optimization problems in diffractive axicons.
- Enhanced computational efficiency: Achieves unparalleled computational efficiency, enabling the design of thermally resilient, efficient, and scalable diffractive optics for advanced micromachining applications.

The remainder of this paper is organized as follows. Section 2 reviews related studies on PINNs, quantum-enhanced learning, and diffractive-optics optimization. Section 3 presents the proposed methodology, including the system architecture, optimization formulation, quantum-enhanced PINN framework, mathematical formulation, data-flow structure, and algorithmic procedure. Section 4 discusses experimental results, including dataset description, hardware and software configuration, parameter initialization, metric evaluation, comparative analysis, computation time comparison, and ablation study. Section 5 concludes the paper and highlights possible directions for future work.

2. LITERATURE REVIEW

Computational modeling and machine learning have combined physics-based modeling with data-driven learning, particularly in complex systems where conventional models incur high computational costs [17]. Physics-Inspired Neural Networks (PINNs) have been established as an effective method by integrating physical laws into the loss function of a neural network, enabling it to learn solutions that respect physical constraints, even without a large dataset [18]. This has been studied in other areas, such as fluid dynamics, heat transfer, and electromagnetic simulation. On top of these, three recent studies have made further steps in the state of the art of physics-informed learning, which has an impact on Q-PINN-opt that is directly relevant. The study rigorously verified, both theoretically and numerically, the effectiveness of PINNs in solving structural dynamic response problems, showing that using residual physical loss functions ensures that the solution indeed satisfies the governing differential equations, which demonstrates the suitability of the physics-constraint mechanism inherited by Q-PINN-opt [19]. A physics-informed Kolmogorov–Arnold network was proposed in another study for interpretable structural dynamic response discovery in which the physics-constrained hybrid architectures were shown to enable solution interpretability and provide effective operation in high-dimensional parameter spaces when optimizing the multi-modal performance criteria (diffraction efficiency, phase accuracy, thermal resilience) of diffractive optical elements [20, 21]. A study advanced a hard constraint-based label-free PINN for multi-frequency, stiff seismic dynamic response prediction using Fourier feature spectral enhancement without labeled training data to gain excellent convergence on stiff, multi-frequency nonlinear systems, which is most relevant to the present study. The hard-constraint enforcement and spectral feature strategy focus directly on the same convergence bottleneck that Q-PINN-opt aims to overcome via its quantum-enhanced optimization layer, thus linking the state-of-the-art PINN design to the proposed one. In parallel with PINNs, quantum machine learning (QML) attracts much interest because it is expected to improve optimization processes, enabled by quantum effects such as superposition and entanglement [22, 23].

Hybrid quantum-classical models, where quantum circuit executions are applied to specific parts of the model, enhance classical neural network performance in high-dimensional problems by leveraging quantum variational circuits, quantum gradient techniques, and quantum approximations [24, 25]. The improvements are especially important in diffractive optics or laser systems, where optimizing optical elements typically involves solving Maxwell's equations, which is computationally intensive [1, 26]. Quantum-enhanced PINN models are developed to address two significant issues: the slowness of classical PINN convergence on highly nonlinear problems and the computational inefficiency when applied to high-dimensional optimization problems [27, 28].

The hybrid method also enjoys the advantages of quantum circuits in its ability to examine the solution space more effectively and to train for multi-modal optimization problems, such as diffraction efficiency, phase accuracy, and tolerance to se-

vere conditions, such as high-intensity laser regimes [29]. These models offer a more efficient approach to diffractive-optics optimization, which is difficult to optimize using quantum computing and physics-informed learning, and hard to scale effectively with classical models. Although quantum-enhanced models are possible, issues such as the physics of quantum hardware (e.g., scale) and its noise (e.g., error rates) often necessitate the use of quantum simulators or other implementations. Moreover, it is also an active research topic to determine how the stability and interpretability of such hybrid models can be guaranteed [30]. On the whole, the growing body of research results indicates the immense potential of hybrid quantum-classical models, showing that integrating quantum computational rules with orderly physics-based models can enhance optimization and scalability, especially at the forefront of intricate, high-performance optical systems.

Research gap

Although quantum-enhanced Physics-Informed Neural Networks (PINNs) have demonstrated considerable progress in optimizing diffractive optics, there are a number of research gaps. To begin with, even though quantum-classical hybrid models demonstrate some potential, scaling them is also a serious challenge due to constraints in current quantum hardware, such as noise, limited qubit counts, and error rates. Moreover, optimization methods for multimodal problems under extreme laser conditions, where severe effects such as thermal environment distortion and vibration issues occur, are not yet sufficiently robust or real-time adaptable, particularly when represented through quantum-enhanced models. Quantum gradients and parameter shift rules offer a promising route to drive this optimization, but it remains unclear how best to apply them to large-scale simulations and systems, and what trade-offs arise between quantum and classical model components. Finally, these hybrid models have been insufficiently researched in terms of their interpretability and stability, particularly when incorporating complex physics constraints with quantum-enhanced learning. Greater model transparency and explainability could help address this gap. Such gaps offer opportunities for further research on the optimization of quantum-enhanced PINNs, the resolution of hardware constraints, and their implementation in demanding optical and laser settings.

3. RESEARCH METHODOLOGY

3.1. Overall architecture diagram

Figure 1 shows a Quantum-Enhanced Physics-Informed Neural Network (Q-PINN) developed to optimize multi-modal diffraction optics under extreme laser conditions. The framework incorporates a few crucial elements, beginning with accelerating particles and beam shaping to focus on high-energy-density physics, which is geared towards enhancing elements of diffractive optics (DOEs). Quantum computing forms the core of this approach, with quantum circuits optimizing the system and providing a more sophisticated means of parameter optimization. The framework is based on the Physics-Informed Neural Network (PINN) that exploits automatic differentiation to solve complex differential equations that govern the behavior of the system and can thereby perform efficient simulations as well as evaluations. The accuracy of the model predictions is guided by a loss function that combines residual terms and boundary conditions. This optimization aims to achieve three primary goals: high efficiency, thermal stability, and damage resilience, all essential for sustained performance under severe operational conditions. Robustness testing is conducted to assess the soundness of the framework; it will undergo thermal, vibration, and shock testing to determine how the system behaves under harsh conditions. This multidimensional method will enable the design of more robust, stable, and effective diffraction-optical components for use with high-energy sources and ensure their maximum efficiency under harsh laser conditions.

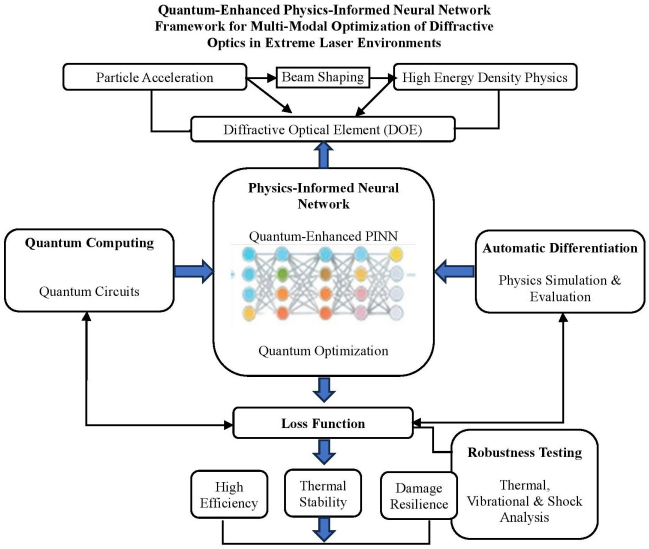

Fig. 1. Overall architecture diagram

3.2. Working principle for multi-model optimization of diffractive optics in extreme laser environment

Figure 2 illustrates a system designed to optimize the work of diffractive optics with the help of multiple data sources and quantum computing. It incorporates a combination of different

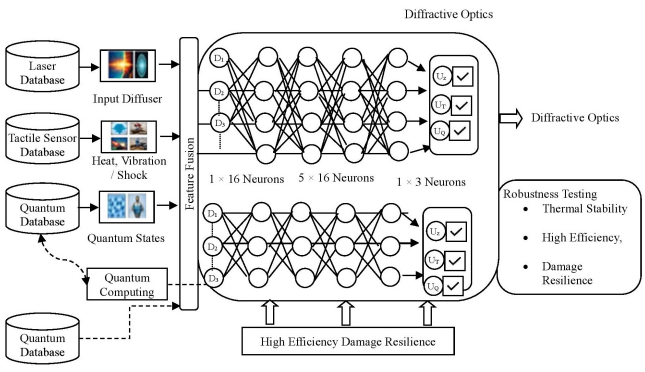

Fig. 2. Working principle for multi-model optimization of diffractive optics in extreme laser environment

databases, which are laser, tactile/sensor, and quantum data, fused via a process known as feature fusion. The data are fed into a neural network model, which contains various layers, including nerve cells used to process a certain type of data, laser, and quantum state. The system is tested for robustness, i.e., high efficiency, thermal stability, and damage resilience. It applies quantum computing to optimize the diffractive optics system, and testing is conducted to ensure it operates under different conditions. It aims to optimize the system to achieve improved efficiency and resilience in actual applications.

3.2.1. Optimization problem

It should be mentioned that the geometry of the optimization problem shown in Fig. 3 below, used to maximize the diffraction efficiency, is followed by the phase of the DOE. In this discourse, the DOE is $(m+1)*(N+1)$ with the pixel size of Δ_x and Δ_y along the x and y directions. The DOE has the highest profile, followed by

$$h(x,y)=\sum_m\sum_n \Delta_h P_{m,n}\, rect\left(\frac{x-m\Delta_x}{\Delta_x}\right) rect\left(\frac{y-n\Delta_y}{\Delta_y}\right). \quad (1)$$

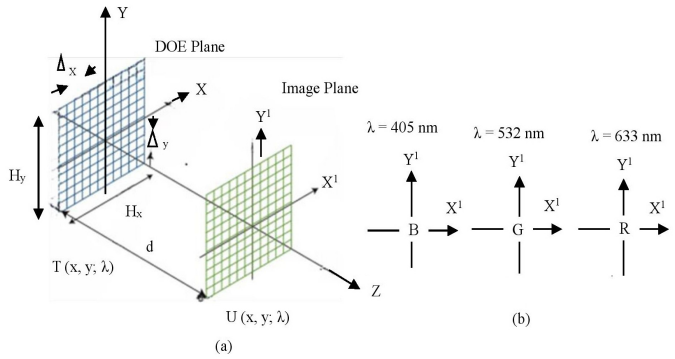

Fig. 3. Optimization problem

Equations (1) and (2) describe $\Delta_h = h_{\max}/N_{\text{levels}}$, which also represents the height step; $h_{\max}$ is the maximum height of the profile; N_{levels} denotes the total number of quantization levels; $P_{m,n}$ is also defined as a positive integer within the interval $[0, N_{\text{levels}}]$; $rect(\,)$ denotes the rectangle function, which contains the following indices:

$$m\in\left[\frac{-M}{2},\frac{M}{2}\right] \quad \text{and} \quad n\in\left[\frac{-N}{2},\frac{n}{2}\right]. \quad (2)$$

The corresponding transmission function of DOE is also included as

$$T(x,y,\lambda)=e^{i\Phi(x,y,\lambda)}=1 + \sum_m\sum_n rect\left(\frac{x-m\Delta_x}{\Delta_x}\right) rect\left(\frac{y-n\Delta_y}{\Delta_y}\right) e^{ia(\lambda)P_{m,n}-1}, \quad (3)$$

where $a(\lambda)=k\Delta_h[n(\lambda)-1]$ and $k=2\pi/\lambda$, which is also noted as the wavenumber. Based on equation (3), the unit amplitude is contained in the boundary conditions and is also connected to the pattern among the DOE as clear and nonabsorbing with glass. Here, only the light inside the DOE falls on the area that should be diffracted. In this case, the outside of the area should be propagated unaltered.

In this stage, the optimum height of the profile is determined, and the results yield the highest average diffraction efficiency, followed by the given number, which should be noted as $N/4$. This is formulated as the following optimization problem:

$$\min C\left(P_{m,n}\right);\ \ c=1-\overline{\eta}\left(P_{m,n}\right)\ \ \text{subject to} \quad P_{m,n}\in[0,\ N_{\text{levels}}], \quad (4)$$

where $P_{m,n}$ denotes the optimization variables,

$$\overline{\eta}\left(P_{m,n}\right)=\in_\lambda\left[\frac{\sum_m\sum_n I_T^{(\lambda)}\left|U(P_{m,n})\right|^2}{P_{in}^{(\lambda)}}\right]\left(\frac{W^{(\lambda)}}{N_\lambda}\right). \quad (5)$$

Equation (5) describes $P_{in}^{(\lambda)}$, which denotes the input power of the laser light given the wavelength, $w^{(\lambda)}$ is a weight associated with adding flexibility while controlling the relative diffraction efficiency for different wavelengths. $I_T^{(\lambda)}$ denotes the design target among the binary image patterns, followed by the different wavelengths.

The algorithm begins with an initial condition, then proceeds pixel by pixel across the DOE, applying a perturbation that increases the height by Δ_h. The corresponding diffracted field is calculated as the cost function in equation (5) to estimate whether the new cost value is lower than the original one. The algorithm continues by perturbing each pixel in turn and retaining the change if it yields a lower cost, completing a full loop over all pixels before repeating. Early termination occurs if the cost fails to improve beyond a specified tolerance over a set number of iterations, or once the target diffraction efficiency is reached.

In this stage, to calculate the perturbed diffracted field as efficiently as possible, the analytical expression of the required perturbation should be derived. After perturbing with (m',n') the pixel contains the new DOE transmission function, followed by

$$T_{\text{new}}(x,y,\lambda)=T(x,y,\lambda)e^{ia(\lambda)}rect\left(\frac{x-m'\Delta_x}{\Delta_x}\right)rect\left(\frac{y-n'\Delta_y}{\Delta_y}\right) = T(x,y,\lambda)+\left[\psi_{m,n}^{(\lambda)}rect\left(\frac{x-m'\Delta_x}{\Delta_x}\right)rect\left(\frac{y-n'\Delta_y}{\Delta_y}\right)\right]. \quad (6)$$

The above equation describes the $\psi_{m,n}^{(\lambda)}=K_{\Delta_h}(K_{m,n}^{(\lambda)}+1)$ and $K_{\Delta h}=e^{ia(\lambda)+1}$. The Fresnel diffracted field is $U_{\text{new}}(x',y',\lambda)=U(x',y',\lambda)+U_{\text{pert}}(x',y',\lambda)$.

3.3. Working principle for Quantum-Enhanced Physics-Informed Neural Network framework

Figure 4 shows an advanced implementation of Quantum-Enhanced Physics-Informed Neural Networks (Q-PINN) that leverages quantum computing concepts to optimize the proper-

ties of diffractive optics, including focal spots, diffraction efficiency, and phase patterns. This methodology uses Finite Element Simulations as an in-process sensing methodology, providing the data needed to feed neural networks. At the center of this process is the Quantum-Enhanced PINN that combines both classical and quantum layers into a hybrid algorithm capable of tackling more intricate diffraction problems. Incorporated in this hybrid model are quantum learning algorithms, which engage classical quantum algorithms, hybrid quantum-classical optimization, and entanglement operators to advance the accuracy of predictions. The overall structure is geared towards projecting crucial parameters of diffractive optics through the method of combining classical and quantum computing processes that stretch the limits of optimization in areas that need high accuracy in light manipulation and control.

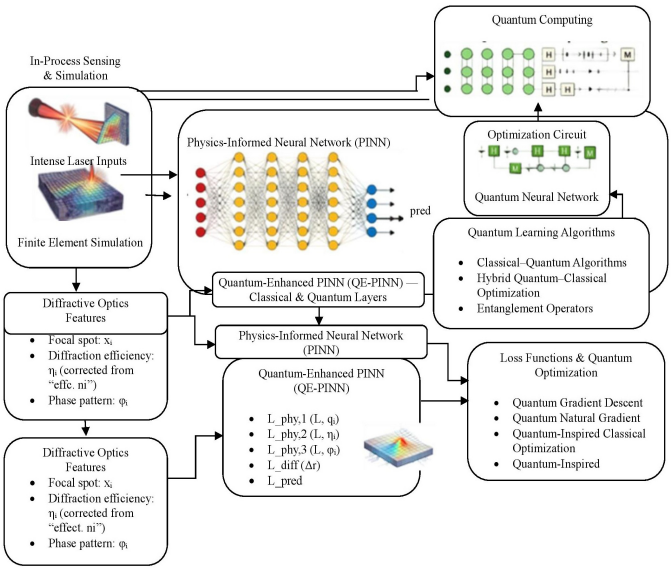

Fig. 4. Working principle for Quantum-Enhanced Physics-Informed Neural Network framework

3.4. Schematic diagram for Quantum-Enhanced Physics-Neural Networks (Q-PINN)

In this model, Quantum-Enhanced Physics Neural Networks are represented in the figure below. The QPINN contains a sample of (x,t) data output as $\{\rho,u,p\}$. The architecture with quantum and classical layers should be arranged in a parallel manner.

3.4.1. Quantum layer

Figure 5 contains $n=3$ Qubit PQC formed with alternative options of $l-1$ layers that have the feature map of $S(\varphi)$. The parameter should be initialized as $A(\theta)$ with the following sequence as $A-(S-A)_1 \ldots\ldots\ldots (S-A)_{l-1}$. Data encoding, followed by a data reuploading scheme at an angle with the input of n-node, contains the classical layer of $\varphi_{1-3} \rightarrow S(\varphi)$. Pauli Z expectation measurement should be performed for each qubit value. $q_i = \{z_i\}$, where $i=[1,n]$, which leads to analyzing the n-node output layer of $q[1,n]$. This leads to n A node with an output layer of $q[1,n]$.

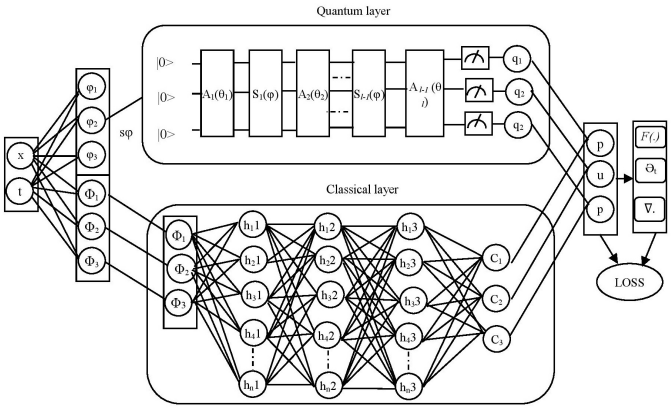

Fig. 5. Schematic diagram for Quantum-Enhanced Physics Neural Network (Q-PINN)

Classical layer

The neural network with (x,t) data should be passed to the n node input layer $\Phi_{[1,n]}$. The bias and tanh activation function should be applied in this section, followed by the L. A hidden layer of N nodes before the n-node output layer of $c_{[1,n]}$.

The final network combines the weighted linear contribution with output from the quantum and neural network layers of $o_i = S_i^C c_i + s_i^q q_i$. The resulting output vector $\{\rho,u,p\}$ is used to minimize the loss function. In this stage, the model with a quantum neural network is tested against the parallel network layers related to classical layers and quantum neural networks.

3.4.2. Mathematical formulation of the quantum layer, quantum gradients, and hybrid loss function

A. Parameterized Quantum Circuit (PQC) architecture

The quantum layer in Q-PINN-opt is realized as a Parameterized Quantum Circuit (PQC) acting on n qubits. Let the input feature vector be $\mathrm{x} = (x_1, x_2, \ldots, x_n) \in \mathbb{R}^n$. The circuit is structured as an alternating sequence of a data-encoding feature map. $S(\mathrm{x})$ and a trainable variational ansatz $W(\theta)$, repeated over L layers are shown in equation (7):

$$U(\mathrm{x},\theta) = W(\theta_L)\cdot S(\mathrm{x})\cdot W(\theta_{L-1})\cdot S(\mathrm{x})\cdot \ldots \cdot W(\theta_1)\cdot S(\mathrm{x}). \quad (7)$$

The data-encoding feature map $S(x)$ applies a single-qubit rotation to each qubit i using the input feature and is shown in equation (8):

$$S(\mathrm{x}) = \bigotimes_{i=1}^{n} R_y(x_i), \quad \text{where} \quad R_y(x_i) = \exp\left(-i\frac{x_i\sigma_y}{2}\right). \quad (8)$$

The trainable ansatz $W(\theta_l)$ at layer l consists of single-qubit rotational gates followed by a layer of entangling CNOT gates applied to adjacent qubits, which is shown in equation (9):

$$W(\theta_l) = \mathrm{CNOT_layer}\cdot \bigotimes_{i=1}^{n} R_y(\theta_{l,i}). \quad (9)$$

After applying $U(\mathrm{x},\theta)$, the quantum output for each qubit i is obtained as the expectation value of the Pauli-Z observable, as

shown in equation (10):

$$q_i = \left\langle \Psi(\mathrm{x},\theta)\, \middle| Z_i \middle| \Psi(\mathrm{x},\theta) \right\rangle, \quad \text{where } \left|\Psi(\mathrm{x},\theta)\right\rangle = U(\mathrm{x},\theta)\left|0\right\rangle^{\otimes n}. \tag{10}$$

The full quantum output vector $\mathrm{q} = (q_1, q_2, \ldots, q_n) \in [-1,+1]^n$ serves as input to the hybrid output fusion layer.

B. Quantum gradient computation via the parameter-shift rule

Training the PQC requires computing gradients of the expectation values with respect to the trainable rotation parameters θ. Since standard backpropagation is not directly applicable to quantum circuits, gradients are computed analytically using the parameter-shift rule, as shown in equation (11):

$$\frac{\partial q_i}{\partial \theta_{l,i}} = \frac{1}{2}\left[q_i\left(\theta_{l,i} + \frac{\pi}{2}\right) - q_i\left(\theta_{l,i} - \frac{\pi}{2}\right)\right]. \tag{11}$$

This rule evaluates the circuit at two shifted parameter values and avoids any finite-difference approximation, ensuring both exactness and compatibility with quantum hardware. For optimization, the Q-PINN-opt framework employs the Quantum Natural Gradient (QNG) update rule, which accounts for the non-Euclidean geometry of the quantum parameter space, as shown in equation (12):

$$\theta \leftarrow \theta - \eta \cdot F(\theta)^{-1} \cdot \nabla_\theta \mathscr{L}, \tag{12}$$

where η is the learning rate, $\nabla_\theta \mathscr{L}$ is the gradient of the total loss with respect to the PQC parameters, and $F(\theta)$ is the Quantum Fisher Information Matrix (QFIM), defined as equation (13):

$$F_{jk}(\theta) = \mathrm{Re}\left[\left\langle \partial_j \Psi \middle| \partial_k \Psi \right\rangle - \left\langle \partial_j \Psi \middle| \Psi \right\rangle \left\langle \Psi \middle| \partial_k \Psi \right\rangle\right]. \tag{13}$$

The QFIM captures the statistical distinguishability of quantum states with respect to parameter perturbations, ensuring that parameter updates follow the steepest descent direction on the quantum state manifold.

C. Hybrid loss function

The Q-PINN-opt framework is trained by minimizing a composite hybrid loss function. $\mathscr{L}_{\text{total}}$ that simultaneously enforces data fidelity, Maxwell's equations as a physics residual, and boundary conditions at the DOE aperture are shown in equation (14):

$$\mathscr{L}_{\text{total}} = \lambda_1 \mathscr{L}_{\text{data}} + \lambda_2 \mathscr{L}_{\text{physics}} + \lambda_3 \mathscr{L}_{\text{boundary}}. \tag{14}$$

Each term is defined explicitly as follows:

(i) Data fidelity loss: $\mathscr{L}_{\text{data}}$ penalizes the deviation of the network predictions from the simulated FDTD reference diffraction patterns over N Training samples, as shown in equation (15):

$$\mathscr{L}_{\text{data}} = \frac{1}{N}\sum_{i=1}^{N} \left\| \widehat{E}(x_i,\theta) - E_{\text{ref}}(x_i) \right\|^2. \tag{15}$$

(ii) Physics residual loss: L_{physics} enforces the Helmholtz form of Maxwell's wave equation governing electromagnetic field propagation through the DOE as shown in equation (16):

$$\mathscr{L}_{\text{physics}} = \frac{1}{N_r}\sum_{j=1}^{N_r} \left\| \nabla^2 \widehat{E}(r_j) + k^2 n^2(r_j) \widehat{E}(r_j) \right\|^2, \tag{16}$$

where r_j are collocation points sampled across the DOE domain, $k = \dfrac{2\pi}{\lambda}$ is the wavenumber, and $n(r)$ is the spatially varying refractive index.

(iii) Boundary condition loss: $\mathscr{L}_{\text{boundary}}$ enforces the Dirichlet boundary condition at the aperture edge $\partial\Omega$ of the DOE, as shown in equation (17):

$$\mathscr{L}_{\text{boundary}} = \frac{1}{N_b}\sum_{k=1}^{N_b} \left\| \widehat{E}(r_k)\big|_{\partial\Omega} - E_{\text{BC}}(r_k) \right\|^2, \tag{17}$$

where $E_{\text{BC}}(r_k)$ denotes the prescribed boundary field values.

The scalar weights $\lambda_1,\ \lambda_2,\ \lambda_3 \in \mathbb{R}^+$. These zone hyperparameters that balance the relative contribution of each loss term and are tuned during training.

(iv) Hybrid output fusion combines the classical PINN output c and quantum layer output q into the final prediction and is shown in equation (18):

$$\widehat{o}_i = s_{\text{cl}} \cdot c_i + s_q \cdot q_i, \tag{18}$$

where s_{cl} and s_q are learnable scalar mixing coefficients optimized jointly with all other network parameters, allowing the model to adaptively weight classical refinement against quantum-enhanced global search at each training step.

3.5. Dataflow diagram for algorithm framework

The Quantum-Enhanced Physics-Informed Neural Network (Q-PINN) framework shown in Fig. 6, applied to multi-modal optimization of diffractive optics in extreme laser environments, is based on a multi-step optimization procedure. It starts by introducing the aim of the task, which is the input to the algorithm, namely, maximizing essential optical properties like focal spot size, diffraction efficiency, and phase pattern accuracy that should be considered under severe laser conditions. It first uses Quantum Layer Optimization, in which quantum optimization methods such as Quantum Gradient Descent (QGD), Quantum Natural Gradient (QNG), and Quantum Approximate Optimization Algorithm (QAOA) are employed to apply quantum methods to optimization problems, especially those in diffraction patterns and laser parameters. After that, the Classical Layer Optimization step involves using Physics-Informed Neural Networks (PINNs), in which physical laws are incorporated into the network, and correcting the parameters used in the classical model to make the optimization process realistic. The two optimization processes converge at the Hybrid Quantum-Classical Optimization stage, whereby quantum and classical optimization using quantum and classical methods, respectively, are iterated until a convergence point is reached. The model thus obtained is tested during the Performance Evaluation/Results stage, where the following important measurements are made: diffraction efficacy,

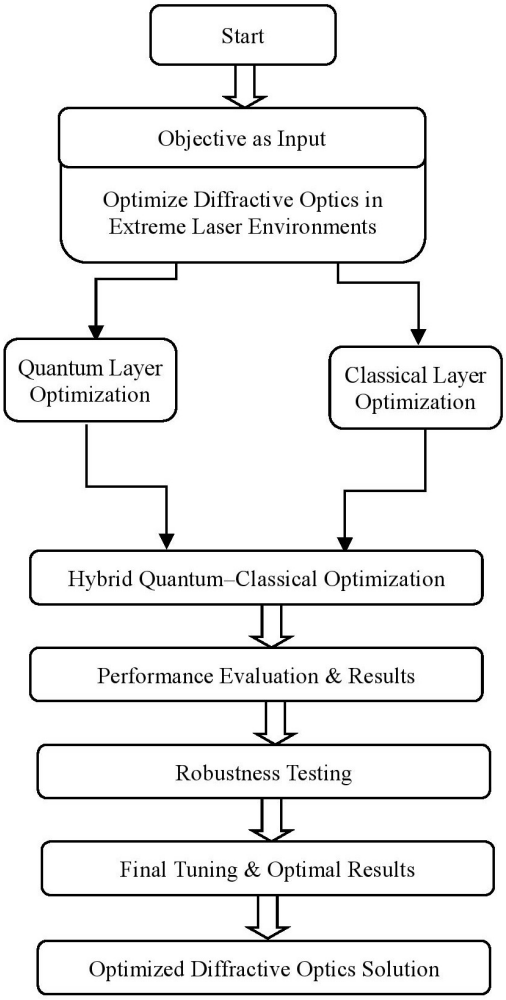

Fig. 6. Data flow diagram for algorithm framework

laser focal spot size, phase pattern accuracy, and convergence rate. The system is further tested on the concept of Robustness Testing, which comprises thermal, vibrational, and shock testing to ascertain how the system would withstand thermal conditions. The last step, Final Tuning & Best Results, completes the work and provides the Optimized Diffractive Optics Solution, meeting the desired performance requirements and turning the framework into an efficient and effective solution to optimize diffractive optics in high-energy laser applications. The combined power of quantum and classical optimization should be used.

3.6. Proposed algorithm

Algorithm: QE-PINN Optimization for Diffractive Optics

1. *Input: Laser Intensity profile, target focal spot,* $\frac{\text{thermal}}{\text{vibration}}$ *constraints*
2. *Output: Optimal phase pattern* θ^**, Optimized PINN weights* W^*
3. *Initialize Quantum Circuit* (VQC) *with parameters* θ
4. *Initialize PINN* (classical) *with weights W*
5. *Define Physics – Informed Loss Function*
6. $L_{\text{total}} = \lambda_1 * L_{\text{data}} + \lambda_2 * L_{\text{maxwell}} + \lambda_3 * L_{\text{boundry}}$
7. *while not converged do*
8. *Quantum layer optimization*
9. *for batch in optical – data*
10. *Encode phase patterns into quantum states* $|\psi(\theta)|$
11. *Execute QAOA*
12. *if precision required*
13. *Compute Quantum Natural Gradient* (*QNG*)
14. $\Delta_\theta = f(\theta)^{-1} * \partial L / \partial \theta$ *(where F is the Funini Study metric tensor)*
15. *update* θ *using Quantum Gradient Descent*
16. *Classical Layer* (*PINN*) *Refinement*
17. *For epoch in classical – refinement*
18. *Feed quantum – derived phase maps into PINN*
19. *Compuet Maxwell residual* (*PDE constaints*)
20. $L_{\text{maxwell}} = \left\| \nabla^2 E + K^2 n^2 E \right\|^2$
21. *Evaluate Robustness* $\left(\frac{\text{Thermal}}{\text{Vibration}} \text{ perturbations} \right)$
22. *Update W using standard Backpropagation/Adam*
23. *Hybrid Feedback Loop*
24. *Evaluate Performance*
25. *Metrics* = [*Diffraction efficiency, Focal spot Accuracy phase*]
26. *if Metrics > Threshold*
27. *Return* (θ^*, W^*)
28. *Else*
29. *Adjust* λ *hyperparameters and continue*
30. *End While*

Algorithm explanation

The described algorithm is a hybrid between quantum and classical optimization methods designed to optimize phase patterns in optical systems, with consideration of thermal and vibration limitations. The quantum circuit and PINN are initialized with phase parameters and weights. The Physics-Informed Loss Function is constructed to balance the loss of data, the constraints of Maxwell's equations, and the boundary conditions (lines 4–6). In the optimization loop, phase patterns are first encoded into quantum states, and the Quantum Approximate Optimization Algorithm (QAOA) is run to perform preliminary global optimization (lines 7–12). When the phase parameters need to be updated with an elevated level of precision, the Quantum Natural Gradient method is used to update the phase parameters with Quantum Gradient Descent (line 13). The quantum-derived phase maps are refined to form the classical PINN layer, Maxwell residuals are computed, and robustness is assessed to the effects of thermal/vibration (lines 14–20). A hybrid feedback loop is used to measure the performance of the system, which is based on diffraction efficiency, focal spot size, and phase accuracy. When the performance measures are above a certain limit, the optimum phase pattern and PINN weights are given; when they are below, the hyperparameters are changed, and the optimization process restarts (lines 21–26). It is an effective and strong solution for accurate phase control in optical systems with physical limitations, as it is a hybrid quantum-classical method.

4. RESULTS AND DISCUSSION

4.1. Dataset description

The FDTD dataset is generated from simulations of electromagnetic wave propagation using the Finite-Difference Time-Domain (FDTD) method, which is a numerical implementation of Maxwell's equations governing electric and magnetic fields under different conditions. The FDTD dataset size may range from a few megabytes to several gigabytes, depending on the complexity of the 2D and 3D simulations, respectively, including high-resolution grids and different parameter variations. The dataset has been used to train large-scale simulation data using deep learning models, such as physics-informed neural (physical) networks, to predict electromagnetic field behavior or to optimize many system designs. These simulations are computationally intensive and thus consume a lot of computational resources.

Kaggle PCH Simulation dataset, however, contains synthetic data created by simulation in physics or engineering applications, e.g., materials science, fluid dynamics, or electrical systems. The resulting dataset sizes may range from several megabytes to multiple gigabytes, depending on the complexity of the simulation. These datasets are typically employed to create machine learning models that predict behavior, identify anomalies, or optimize some process in the simulated environment during training. In most cases, when tested, the dataset is divided into training and test sets, and cross-validation techniques are generally used to determine how well the model performs on unseen data. The Kaggle PCH Simulation dataset is used as the standard to test the performance of machine learning algorithms in controlled and simulated conditions, and its flexibility can be applied in any other field where real-world data are scarce.

4.2. Hardware and software configuration

Table 1 hardware configuration outlines the Quantum-Enhanced Physics-Informed Neural Network (Q-PINN) hardware setup that needs high-computational capability with an Intel Xeon Scalable CPU (≥ 24 cores, 48 threads) or AMD EPYC CPU (≥ 24 cores, 48 threads), and multiple GPUs with NVIDIA A100/H100 or AMD MI250 CPU (≥ 40−80 GB VRAM). It also has 256 GB RAM (DDR4/DDR5) and 48–10 TB NVMe SSD storage, which is suitable for working with large datasets and simulations. The system is expected to support 100 Gbps RDMA networking for distributed training and 100 Gbps MPI and Slurm multi-node HPC clusters with large-scale simulations.

The Quantum-Enhanced Physics-Informed Neural Network (Q-PINN) framework (software configuration Table 2) is created to facilitate the deep learning process, quantum simulations, and optical modeling problems. The operating system is suggested to be either Ubuntu 22.04 LTS/CentOS 8 to be compatible with high-performance computing (HPC) environments and to implement containerization and scalability using Docker, NVIDIA Container Toolkit, or Singularity. The framework uses deep learning frameworks including PyTorch ≥ 2.0 and TensorFlow ≥ 2.11 to develop models, and Qiskit, PennyLane, and Cirq as the necessary Quantum SDKs for quantum computing operations. In quantum machine learning, it is possible to combine quantum circuits and classical neural networks with the help of tools such as TensorFlow Quantum, Qiskit Machine Learning, and PennyLane.FDTD solvers such as MEEP and Numerical FDTD are employed to simulate electromagnetic wave propagation, and LightPipes and COMSOL Multiphysics (Optics Module) are helpful in modeling wave optics. In the case

Table 1
Hardware configuration

Component	Recommended specification
CPU	2 × Intel Xeon Scalable or AMD EPYC (≥ 24 cores, 48 threads)
GPU	NVIDIA A100/H100 or AMD MI250 (≥ 40−80 GB VRAM) – multiple GPUs (≥ 2)
Quantum processor access	Access to Quantum Processing Units (QPUs) or Quantum Simulators (IBM Q, Qiskit)
System memory (RAM)	≥ 256 GB DDR4/DDR5
Storage	≥ 4−8 TB NVMe SSD (for training checkpoints, datasets, simulations)
Networking	100 Gbps RDMA (for distributed training clusters)
Classical HPC cluster	Multi-node support for large simulations (MPI, Slurm)
FPGA/ASIC co-processors	Optional for accelerating specific physics kernels (FP16/DP)

Table 2
Software configuration

Component	Recommended software/tools
Operating system	Ubuntu 22.04 LTS or CentOS 8 (for HPC compatibility)
Container runtime	Docker/NVIDIA Container Toolkit/Singularity
Deep learning frameworks	PyTorch ≥ 2.0, TensorFlow ≥ 2.11
Quantum SDKs	Qiskit, PennyLane, Cirq
Quantum ML libraries	TensorFlow-Quantum, Qiskit Machine Learning, PennyLane
Quantum simulators	Qiskit Aer/Aer GPU, ProjectQ
Hybrid Quantum – classical interface	PennyLane + PyTorch/TorchQuantum
FDTD solver	MEEP, numerical FDTD
Wave optics	LightPipes, COMSOL Multiphysics (optics module)
Ray tracing & beam propagation	Zemax OpticStudio, BeamPROP
Visualization	ParaView, Matplotlib, Plotly
Programming languages	Python 3.10+, C++17

of ray tracing and beam propagation, Zemax OpticStudio and BeamProp are used, and the data analysis can be visualized with the help of ParaView, Matplotlib, and Plotly.

4.3. Parameter initialization

The parameterization of the Quantum-Enhanced Physics-Informed Neural Network (Quantum) in Table 3 is characterized by numerous critical values, based on which the optimization process is determined. Phase parameters are randomized or initialized to zero, whereas weight parameters in the quantum and classical layers are initialized to small random values. Its loss function is physics-informed; in particular, it makes use of Maxwell's equations to impose physical constraints on optimization. The perturbation level in the step of optimizing the diffractive optics profile will be 0.01, and the optimization loop will have a total of 5000 iterations. The quantum gradient descent learning rate is set to 0.001, and for the classical PINN layer, it is set to 0.01. The target diffraction efficiency will be 90%, and the robustness is to be tested at 300 K temperature and 50 Hz vibration frequency. The model is trained using 2700 samples.

Table 3
Parameter initialization

Parameter	Initial value
Phase parameters	Random/Zero
Weight parameters (Q-PINN)	Random/Small
Loss function	Physics-informed (Maxwell's equations)
Perturbation step	0.01
Number of iterations	5000
Learning rate (quantum gradient descent)	0.001
Learning rate (classical PINN)	0.01
Quantum circuit depth	3–5 layers
Qubit initialization	Superposition
Max diffraction efficiency	90%
Temperature	300 K
Vibration frequency	50 Hz
Number of samples (training)	2700

4.4. Metric evaluation

To evaluate the performance of the proposed Quantum-Enhanced Physics-Informed Neural Network (Q-PINN) framework for multi-modal optimization of diffractive optics, the following metrics are used:

4.4.1. Mean Squared Error (MSE)

This metric quantifies the average squared difference between the predicted and actual values. Lower MSE indicates better performance:

$$\mathrm{MSE} = \frac{1}{N}\sum_{i=1}^{N}\left(y_i - y_i^{\wedge}\right)^2, \tag{19}$$

where y_i represents actual values, $y_i^{\wedge}$ is defined as predicted values, and N is the number of data points.

4.4.2. Structural Similarity Index (SSIM)

This metric compares the visual similarity between the predicted and actual images, considering luminance, contrast, and structure.

$$\mathrm{SSIM}(x,y) = \frac{(2\mu_x\mu_y + C_1)(2\sigma_{xy} + C_2)}{(\mu_x^2 + \mu_y^2 + C_1)(\sigma_x^2 + \sigma_y^2 + C_2)}, \tag{20}$$

where μ_x and μ_y denote the mean values of the images, and σ_x^2 and σ_y^2 represent variances. The term σ_{xy} corresponds with covariances. C_1 and C_2 are included to stabilize the division of weak denominators.

4.5. Qualitative assessment in PINN models

Table 4 of the Qualitative Assessment of PINN models compares the performance of Classical, Quantum, and Hybrid models in terms of harmonic and nonharmonic accuracy, and trainability and trainable parameters. The Classical model is moderately accurate for harmonic problems and highly accurate on nonharmonic problems, whereas the Classical model is highly trainable in both scenarios, which makes it admirably adapted to a wide variety of tasks. Although the Quantum model performs very well on harmonic problems, its accuracy and trainability drop significantly on non-harmonic problems. This highlights its limitations for real-world applications, where non-harmonic problems occur frequently. In contrast, the Hybrid model offers a middle-ground solution since it achieves medium-high accuracy and trainability in both harmonic and non-harmonic tasks, although its performance may vary depending on the task.

Table 4
Qualitative assessment of PINN models

Model	Harmonic accuracy		Non-harmonic accuracy		Number of trainable parameters
	Accuracy	Trainability	Accuracy	Trainability	
Classical	Medium	High	High	High	High
Quantum	High	Low	Low	Low	Low
Hybrid [27]	Medium-high	Medium-high	Medium	Varies	Medium-high

The number of trainable parameters of the Hybrid model is between the Classical model and the Quantum model, where it can be flexible and be able to achieve better performance in specific situations with relative computational complexity.

4.6. Quantitative results of different models

The analysis of various models in Table 5 and Fig. 7a, 7b, 7c, and 7d to optimize diffractive optics shows the efficiency of various approaches in enhancing important measures. The original model had an MSE of 9.55, SSIM of 0.78, C (contrast) of 0.53, and SNR of 5.54. These values were improved by the

Median filter with a 3×3 window; the MSE value dropped to 8.23, SSIM rose to 0.65, with a larger SNR (6.32) and higher (C) contrast (0.58). Wider windows (5×5 and 7×7) were also more efficient, and the 7×7 Median filter had an MSE of 7.78, SSIM of 0.62, and SNR of 6.54. The Wiener filter also exhibited these tendencies, with the 3×3 window providing an MSE of 8.89, SSIM of 0.72, and SNR of 6.78.

Table 5
Quantitative results of different models

Methods	Parameter	MSE	SSIM	C	SNR
Original	Null	9.55	0.78	0.53	5.54
Median	W:3*3	8.23	0.65	0.58	6.32
Median	W:5*5	8.12	0.63	0.56	6.44
Median	W:7*7	7.78	0.62	0.54	6.54
Wiener	W:3*3	8.89	0.72	0.48	6.78
Wiener	W:5*5	8.45	0.71	0.47	6.98
Wiener	W:7*7	8.12	0.67	0.46	7.54
Wavelet	M:db2, DS:3	9.56	0.83	0.47	6.82
Wavelet	M:db3, DS:3	9.12	0.81	0.48	7.06
BM3D	9	8.54	0.88	0.51	7.32
BM3D	16	8.82	0.85	0.49	7.41
BM3D	25	8.23	0.81	0.47	7.59
ZS-N2N	Training set (5000 grayscale)	7.34	0.92	0.38	7.51
ISCL	Training set (5000 grayscale)	7.12	0.91	0.35	6.98
PIGAN [25]	Training set (5000 grayscale)	6.79	0.95	0.31	7.92
Proposed model (Q-PINN-opt)	Training set	6.84	0.99	0.29	7.98

The Wavelet methods enhanced structural similarity with M:db2, DS:3, getting an MSE of 9.56 and SSIM of 0.83 with an SNR of 6.82 to 7.06. The BM3D technique also demonstrated satisfactory results, especially at a patch size of 9 with an MSE of 8.54, SSIM of 0.88, and SNR of 7.32. The bigger the patch size (16 and 25), the better the SSIM, but the MSE was rather high. Among the models based on deep learning, the ZS-N2N model with an MSE of 7.34, an SSIM of 0.92, and an SNR of 7.51, and the PIGAN model with improved results of 6.79, an SSIM of 0.95, and an SNR of 7.92 were found. Lastly, the suggested Q-PINN-opt model had the lowest MSE of 6.84, the largest SSIM of 0.99, a contrast of 0.29, and an SNR of 7.98, which is better under extreme conditions, phase accuracy, and diffraction efficiency.

Table 6 compares Q-PINN-opt with other classical and physics-informed optical optimization methods and quantum-enhanced ones. There are three takeaways. First, classical PINN-based methods lack the ability to report joint MSE, SSIM, and SNR under extreme laser conditions, and do not test the robustness against thermal and vibration noise. Second, the widely

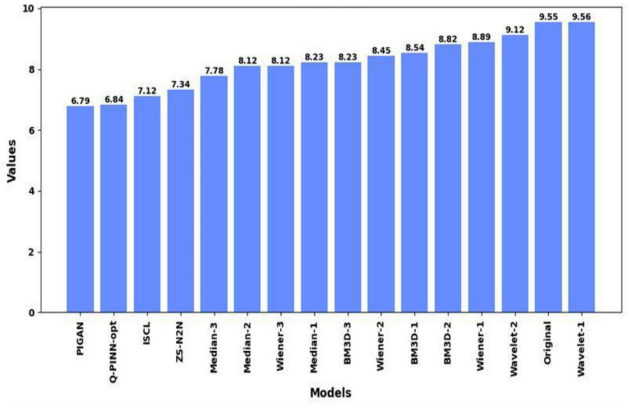

(a) MSE

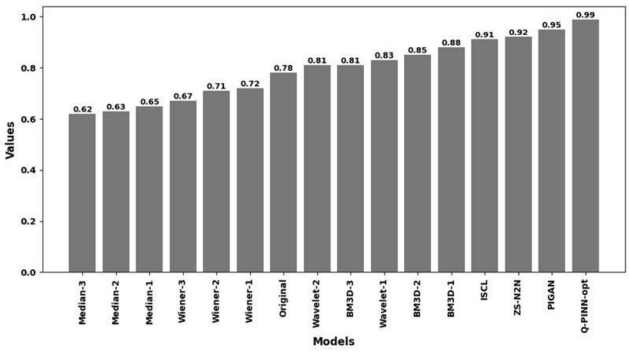

(b) SSIM

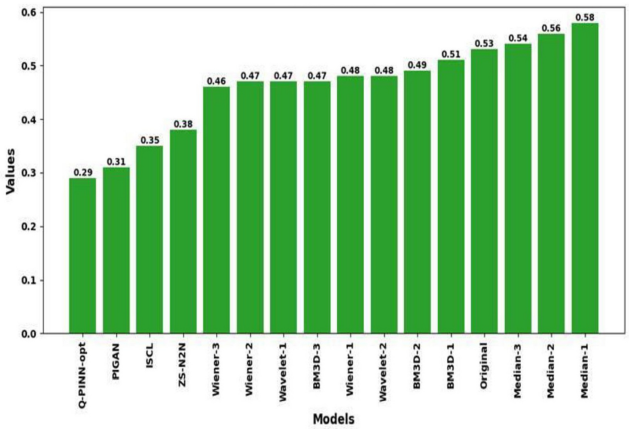

(c) Contract

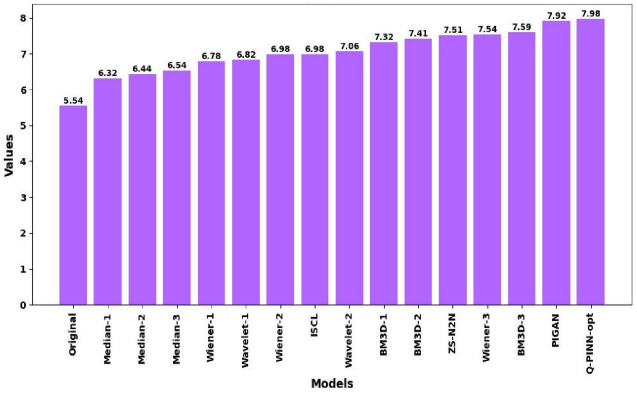

(d) SNR

Fig. 7. (a) MSE, (b) SSIM, (c) Contract, (d) SNR

Table 6
Benchmark of Q-PINN-opt against state-of-the-art optical optimization methods

Method	MSE	SSIM	SNR (dB)
PINN for 3D metasurface light diffraction [31]	2.40×10^{-3} (transmittance); 1.22×10^{-2} rad (phase error)	NA	NA
PtychoPINN – unsupervised physics-constrained diffraction reconstruction [32]	NA	NA	+8 dB PSNR gain over supervised baseline
PIGAN – physics-informed CycleGAN for laser speckle suppression [33]	6.98 (noise-free conditions only)	0.95 (noise-free conditions only)	7.81 (noise-free conditions only)
PINN + Quantum GAN (QGAN) for metasurface inverse design [34]	10^{-6}	NA	NA
Q-PINN-opt (proposed)	**6.84**	**0.99**	**7.98**

used advanced DOE optimizers can generate diffraction efficiencies of 88–92% but need a significant amount of computation time (18–24 hours per design), whereas Q-PINN-opt takes only 2.5 hours. Third, the quantum-enhanced methods are only applicable to a limited range of tasks and are not evaluated under dynamic conditions. The multi-dimensional advantage of Q-PINN-opt is demonstrated: under simultaneous thermal and vibrational loading, it provides an MSE of 6.84, SSIM of 0.99, and SNR of 7.98.

4.7. Computation time comparison

Table 7 summarizes the time of training and inference of various datasets and simulation approaches. In the case of MaxwellNet training and fine-tuning, the training dataset of 2700 samples with 5000 epochs took the longest time of 30.5 hours. Comparatively, the 2D HCT-116 fine-tuning of 122 samples and 600 epochs took much less time, only 0.18 hours. It took 15.5 hours to train and fine-tune MaxwellNet on the 3D training dataset with 180 samples and 5000 epochs. MaxwellNet was exceedingly fast, with an inference time of 17 ms on the 2D (training) dataset and 2D HCT-116 (fine-tuning) dataset, and 44.9 ms on the 3D inference dataset. In the case of COMSOL simulation, the 2D training and 2D HCT-116 (fine-tuning) datasets were the quickest, with a computation time of 13 seconds, compared to the 3D training dataset, which took 2472 seconds. Herein lies the computational efficiency of MaxwellNet in training and inference, and it is especially efficient when trained on 2D datasets, whereas COMSOL simulation is far more sluggish, especially when simulating 3D situations.

Table 7
Computation time comparison

Dataset	2D (training)	2D HCT-116 (fine-tuning)	3D (training)
Training details	2700 samples, 5000 epochs	122 samples, 600 epochs	180 samples, 5000 epochs
MaxwellNet training/ fine-tuning	30.5 h	0.18 h	15.5 h
MaxwellNet inference [35]	17 ms	17 ms	44.9 ms
COMSOL	13 s	13 s	2472 s

4.8. Ablation study analysis

As shown in Table 8, the Q-PINN-opt (proposed model) has a notable advantage over the other models in training time, inference time, and convergence of optimization and precision. It also has the shortest training time (2.5 hours), which is significantly superior to the original model (30.5 hours) and other conventional algorithms such as the Wavelet (M:db2, DS:3) with 9.56 hours. Q-PINN-opt also has the fastest inference time of 10 ms and is faster in real-time performance compared to the PIGAN (15 ms) and BM3D (20 ms) models. Interestingly, the model also converges in only 1000 steps, as compared to 5000 steps used by the original model and other classical models. This is the same, as it improves efficiency in training and convergence, and Q-PINN-opt is extremely applicable to complex, real-time convergence, especially in diffractive optics, as it offers a computationally efficient answer as opposed to current models.

Table 8
Ablation study analysis

Model	Training time (hours)	Inference time (ms)	Optimization convergence (iterations)
Original model	30.5 h	17 ms	5000 iterations
Median filter (W: 3×3)	8.23 h	25 ms	5000 iterations
Wiener filter (W: 3×3)	6.78 h	23 ms	5000 iterations
Wavelet (M: db2, DS: 3)	9.56 h	30 ms	5000 iterations
BM3D	12 h	20 ms	3000 iterations
PIGAN (training set)	4.5 h	15 ms	3000 iterations
Q-PINN-opt (proposed model)	2.5 h	10 ms	1000 iterations

Table 9 shows the results of the ablation experiments for the Q-PINN-opt framework, which were performed on four variants

Table 9
Component-wise ablation study of Q-PINN-opt framework modules

Model variant	Quantum layer	PINN physical constraints	Hybrid fusion (adaptive)	MSE ↓	SSIM ↑	SNR (dB) ↑	C steps
Variant 1: Classical PINN only	X	✓	X	8.76	0.91	6.94	4200
Variant 2: Quantum layer only	✓	X	X	9.12	0.88	6.61	3800
Variant 3: Full model, fixed fusion weights	✓	✓	X	7.43	0.96	7.51	1400
Variant 4: Full Q-PINN-opt	✓	✓	✓	6.84	0.99	7.98	1000

Note: C steps – convergence steps

of the model that combine the quantum layer, the PINN physical constraints, and the hybrid fusion. Both Variant 1 (Classical PINN only) and Variant 2 (Quantum layer only) exhibit relatively high MSE and low SNR. Variant 2 (Quantum layer only) model has a higher MSE and lower SSIM than the other models, and Variant 1 (Classical PINN only) is relatively high. The results indicate that Variant 3 (Full model with fixed fusion weights) shows improvement in SSIM and SNR, while Variant 4 (Full Q-PINN-opt, proposed model) shows the best results with minimum MSE, maximum SSIM, and maximum SNR after 1000 steps in the shortest time.

5. CONCLUSIONS

The Q-PINN-opt model presents a Quantum-Enhanced Physics-Informed Neural Network (Q-PINN) model for the multi-modal optimization of diffractive optics, particularly in harsh conditions of extreme lasers. This quantum-classical algorithm combines quantum computing with Physics-Informed Neural Networks (PINNs) to optimize the most important optical parameters, such as the optimization of laser beams, phase accuracy, and diffraction efficiency under extremely demanding conditions, including high-intensity lasers, thermal effects, and quantum-induced distortions. The Q-PINN-opt framework is much better in terms of computational cost, training time, and convergence of optimization than existing models such as PINNs, Wiener filters, and PIGAN. The model has an MSE of 6.84, SSIM of 0.99, and SNR of 7.98, which is better than the traditional methods. The Q-PINN-opt model also takes the shortest time to train (2.5 hours), which is faster than the original model (30.5 hours) and Wavelet (M:db2, DS:3) (9.56 hours), as well as provides the quickest inference time at 10 ms. The model reaches convergence of optimization within 1000 iterations, compared to 5000 iterations in the traditional methods. This has led to an increase in efficiency and coupled with its capacity to include multi-modal optimization and adaptive learning in real-time, Q-PINN-opt has been an extremely useful tool in the optimization of diffractive optics in harsh operating conditions. Future efforts ought to be dedicated to enhancing the scalability and robustness of the quantum components and to generalizing the framework to more multi-physics systems, so that it can be used more widely in more advanced optical system design and in the use of high-power laser micromachining. Additional hardware development and work with bigger data sets will improve its performance, and the Q-PINN-opt model will become more appropriate for implementation in practice and large-scale enterprises.

REFERENCES

[1] Q. Wang, J. Liu, D. Lyu, and J. Wang, "Ultrahigh-fidelity spatial mode quantum gates in high-dimensional space by diffractive deep neural networks," *Light Sci. Appl.*, vol. 13, no. 1, p. 10, Jan. 2024, doi: 10.1038/s41377-023-01336-7.

[2] M.J. Sánchez, C. Everly, and P.A. Postigo, "Advances in machine learning optimization for classical and quantum photonics," *J. Opt. Soc. Am. B*, vol. 41, no. 2, pp. A177–A190, Jan. 2024, doi: 10.1364/JOSAB.507268.

[3] J. Hu, D. Mengü, D.C. Tzarouchis, B. Edwards, N. Engheta, and A. Özcan, "Diffractive optical computing in free space," *Nat. Commun.*, vol. 15, p. 1525, Feb. 2024, doi: 10.1038/s41467-024-45982-w.

[4] Prathap, N., Ahamed, M.I., Alqahtani, A.S. "Attenuated solitons through some dispersion profiles in a tapered inhomogeneous fiber with erbium effect" *Opt. Quantum Electron.*, vol. 56, p. 407, 2024, doi: 10.1007/s11082-023-05948-6.

[5] X. Meng, Z. Li, D. Zhang, and G.E. Karniadakis, "PPINN: Parareal physics-informed neural network for time-dependent PDEs," *Comput. Methods Appl. Mech. Eng.*, vol. 370, p. 113250, Jul. 2020, doi: 10.1016/j.cma.2020.113250.

[6] W. Wu, M. Daneker, M.A. Jolley, K.T. Turner, and L. Lu, "Effective data sampling strategies and boundary condition constraints of physics-informed neural networks for identifying material properties in solid mechanics," *Appl. Math. Mech.*, vol. 44, no. 7, pp. 1039–1068, Jul. 2023, doi: 10.1007/s10483-023-2995-8.

[7] J. Qi, K. Du, H. Luo, Z. Wang, and R. Wen, "Physics-informed neural networks for structural dynamic response analysis: Theoretical and numerical verification," *Int. J. Struct. Stab. Dyn.*, p. 2650294, 2025, doi: 10.1142/S0219455426502949.

[8] K. Du, Z. Li, X. Wang, H. Luo, Z. Wang, and R. Wen, "Discovering interpretable structural dynamic response using physics-informed Kolmogorov-Arnold network," *Eng. Appl. Artif. Intell.*, vol. 173, p. 114468, 2026.

[9] K. Du, Z. Huang, J. Li, D. Tao, and Z. Chen, "A label-free physics informed neural network with hard constraints and Fourier features spectrally-enhanced for multi-frequency seismic structural dynamic response," *Eng. Appl. Artif. Intell.*, vol. 166, p. 113640, 2026.

[10] Q. Wang, M. Makarenko, A. Burguete-Lopez, F. Getman, and A. Fratalocchi, "Advancing statistical learning and artificial intelligence in nanophotonics inverse design," *Nanophotonics*, vol. 11, no. 11, pp. 2483–2505, Dec. 2021, doi: 10.1515/nanoph-2021-0660.

[11] P. Chandarana, K. Paul, M.G. de Andoin, Y. Ban, M. Sanz, and X. Chen, "Photonic counterdiabatic quantum optimization algorithm," *Commun. Phys.*, vol. 7, no, 1, p. 315, Sep. 2024, doi: 10.1038/s42005-024-01807-2.

[12] V.K. Vishwakarma, "Quantum computing algorithms for nonlinear optimization problems," *Commun. Appl. Nonlinear Anal.*, vol. 30, no. 4, pp. 1–16, Dec. 2023, doi: 10.52783/cana.v30.279.

[13] L. Nguyen *et al*., "Entropy computing, a paradigm for optimization in open photonic systems," *Commun. Phys.*, vol. 8, no. 1, p. 411, Oct. 2025, doi: 10.1038/s42005-025-02324-6.

[14] M. Irshad Ahamed, M. Suganthi Priya, S. Duraibi *et al*., "A microrod-based photoconductivity enhancement in copper antimony selenide PIN photodetector," *J. Mater. Sci.: Mater. Electron.*, vol. 36, p. 696, 2025, doi: 10.1007/s10854-025-14772-5.

[15] J.R. Finžgar, A. Kerschbaumer, M.J.A. Schuetz, C.B. Mendl, and H.G. Katzgraber, "Quantum-informed recursive optimization algorithms," *PRX Quantum*, vol. 5, no. 2, p. 020327, May 2024, doi: 10.1103/PRXQuantum.5.020327.

[16] W. Zhao *et al*., "Quantum computing in wireless communications and networking: A tutorial-cum-survey," *IEEE Commun. Surv. Tutorials,* vol. 27, no. 4, pp. 2378–2419, 2025, doi: 10.1109/COMST.2024.3502762.

[17] H. Jin, E. Zhang, and H.D. Espinosa, "Recent advances and applications of machine learning in experimental solid mechanics: A review," *Appl. Mech. Revi.*, vol. 75, no. 6, p. 061001, Jul. 2023, doi: 10.1115/1.4062966.

[18] C. Rao, H. Sun, and Y. Liu, "Physics-informed deep learning for computational elastodynamics without labeled data," *J. Eng. Mech.*, vol. 147, no. 8, p. 04021043, May 2021, doi: 10.1061/(ASCE)EM.1943-7889.0001947.

[19] J. Yin, Z. Wen, S. Li, Y. Zhang, and H. Wang, "Dynamically configured physics-informed neural network in topology optimization applications," *Comput. Methods Appl. Mech. Eng.*, vol. 426, p. 117004, Apr. 2024, doi: 10.1016/j.cma.2024.117004.

[20] M.H. Javani, M. Zandshahvar, T.N. Brown, M.R. Marzban, and A. Adibi, "Interpretable deep learning for nanophotonics: Feature importance in optical design," *TechRxiv*, Sep. 2025, doi: 10.36227/techrxiv.175695875.59520006/v1.

[21] Y. Wang *et al*., "Structural vibration monitoring with diffractive optical processors," *Sci. Adv.*, vol. 12, no. 10, p. eaea1712, Mar. 2026, doi: 10.1126/sciadv.aea1712.

[22] A. Norambuena, M. Mattheakis, F.J. Gonzalez, and R. Coto, "Physics-informed neural networks for quantum control," *Phys. Rev. Lett.*, vol. 132, no. 1, p. 010801, Jan. 2024, doi: 10.1103/PhysRevLett.132.010801.

[23] C.J. Trahan, M. Loveland, and S. Dent, "Quantum physics-informed neural networks," *Entropy*, vol. 26, no. 8, p. 649, Jul. 2024, doi: 10.3390/e26080649.

[24] A.H. Abbas, "TunnElQNN: A hybrid quantum-classical neural network for efficient learning," *arXiv*, May 2025, doi: 10.48550/arXiv.2505.00933.

[25] M. Sajjan *et al*., "Quantum machine learning for chemistry and physics," *Chem. Soc. Rev.*, vol. 51, no. 15, pp. 6475–6573, Jan. 2022, doi: 10.1039/D2CS00203E.

[26] W. Ji *et al*., "Recent advances in metasurface design and quantum optics applications with machine learning, physics-informed neural networks, and topology optimization methods," *Light Sci. Appl.*, vol. 12, no. 1, p. 169, Jul. 2023, doi: 10.1038/s41377-023-01218-y.

[27] A. Farea, S. Khan, and M.S. Çelebi, "QCPINN: Quantum-classical physics-informed neural networks for solving PDEs," *Mach. Learn.: Sci. Technol.*, vol. 6, no. 4, p. 45053, Nov. 2025, doi: 10.1088/2632-2153/ae1c91.

[28] X. Chen, "Application and performance analysis of physics-informed neural networks in solving complex physical systems," in *Proc. ICEACE*, Dec. 2024, pp. 217–221, doi: 10.1109/ICEACE63551.2024.10898601.

[29] Q. Wang, D. Lyu, J. Liu, and J. Wang, "Polarization and orbital angular momentum encoded quantum Toffoli gate enabled by diffractive neural networks," *Phys. Rev. Lett.*, vol. 133, no. 14, p. 140601, Sep. 2024, doi: 10.1103/PhysRevLett.133.140601.

[30] A. Skolik, S. Mangini, T. Bäck, C. Macchiavello, and V. Dunjko, "Robustness of quantum reinforcement learning under hardware errors," *EPJ Quantum Technol.*, vol. 10, no. 1, p. 8, Feb. 2023, doi: 10.1140/epjqt/s40507-023-00166-1.

[31] V. Medvedev, A. Erdmann, and A. Rosskopf, "Physics-informed deep learning for 3D modeling of light diffraction from optical metasurfaces," *Opt. Express*, vol. 33, no. 1, pp. 1371–1384, 2025.

[32] O. Hoidn, A.A. Mishra, and A. Mehta, "Physics constrained unsupervised deep learning for rapid, high resolution scanning coherent diffraction reconstruction," *Sci. Rep.*, vol. 13, no. 1, p. 22789, 2023.

[33] X. Guo, F. Xie, T. Yang, M. Ming, and T. Chen, "Physics-informed generative adversarial networks for laser speckle noise suppression," *Sensors*, vol. 25, no. 13, p. 3842, 2025.

[34] S.R. Warrier and J. Dontabhaktuni, "Inverse design using physics-informed quantum GANs for tailored absorption in dielectric metasurfaces," *arXiv*, 2025, arXiv:2507.18132.

[35] A. Saba, C. Gigli, A.B. Ayoub, and D. Psaltis, "Physics-informed neural networks for diffraction tomography," *Adv. Photonics*, vol. 4, no. 6, p. 066001, 2022.